Effectively one-dimensional phase diagram of CuZr liquids and glasses

Laura Friedeheim , Nicholas P. Bailey , and Jeppe C. Dyre [*]

"Glass and Time," IMFUFA, Department of Science and Environment, Roskilde University, P.O. Box 260, DK-4000 Roskilde, Denmark

This paper presents computer simulations of Cu_xZr_{100-x} ($x = 36, 50, 64$) in the liquid and glass phases. The simulations are based on the effective-medium theory potentials. We find good invariance of both structure and dynamics in reduced units along the isomorphs of the systems. The state points studied involve a density variation of almost a factor of 2 and temperatures going from 1500 K to above 4000 K for the liquids and from 500 K to above 1500 K for the glasses. For comparison, results are presented also for similar temperature variations along isochores, showing little invariance. In general for a binary system the phase diagram has three axes: composition, temperature, and pressure (or density). When isomorphs are present, there are effectively only two axes, and for a fixed composition there is just one. We conclude that the liquid and glass parts of the thermodynamic phase diagram of this metallic glass former at a fixed composition are effectively one-dimensional in the sense that many physical properties are invariant along the same curves, implying that in order to investigate the phase diagram, it is only necessary to go across these curves.

I. INTRODUCTION

Metallic systems constitute a very important category of glass formers due to their potential applications, as well as their suitability as model systems for studies of the glass transition in computer simulations [1–5]. A well-studied example is the CuZr system, which at certain compositions is a good glass former despite consisting of just two elements [3,6]. This paper presents numerical evidence that both above and below the glass transition, CuZr systems are simpler than has hitherto been recognized. Specifically, for three different compositions of the CuZr system we show that curves exist in the thermodynamic phase diagram along which the atomic structure and dynamics are invariant to a good approximation. The implication is that the two-dimensional thermodynamic phase diagram is effectively one-dimensional in regard to many material properties.

The background of the investigation is the following. In liquid-state theory, a simple liquid is traditionally defined as a single-component system of particles described by classical Newtonian mechanics and interacting by pair-potential forces [7–12]. It has been known for more than half a century that the hard-sphere (HS) model reproduces well the physics of many simple liquids, both in regard to the radial distribution function (RDF) and to dynamic properties such as the viscosity or the diffusion coefficient [12–18]. The traditional explanation of the success of the HS model is the "van der Waals picture," according to which the repulsive forces dominate the physics of simple liquids [12,15–17,19].

The HS model is a caricature simple liquid with pair forces that are zero except right at the particle collisions. In the HS model, temperature plays only the trivial role of

determining particle velocities and thus the timescale; temperature is entirely unrelated to the geometry of relative particle positions. This implies that the thermodynamic phase diagram of the HS system is effectively one-dimensional with density being the only nontrivial variable: the dynamics of two different HS systems with the same packing fraction but different temperatures are identical, except for a trivial uniform scaling of the space and time coordinates. As a consequence, scaled RDFs are identical, scaled mean-square displacements are identical, viscosities are trivially related, etc.

The mapping of a simple liquid to a HS system presents the issue of identifying the effective HS packing fraction at a given thermodynamic state point of the liquid. Many suggestions have been made for how to calculate the relevant hard-sphere radius, yet no consensus has been arrived at [20–28]. Already in 1977, Rosenfeld suggested a powerful thermodynamics-based alternative by basically reasoning as follows [29]: Since the HS packing fraction determines the configurational part of the entropy, this quantity provides the required mapping between a simple liquid and its corresponding HS system. Defining the excess entropy S_{ex} as the system's entropy minus that of an ideal gas at the same density and temperature [12,29], S_{ex} quantifies the configurational entropy (note that $S_{ex} < 0$ because any system is less disordered than an ideal gas). Rosenfeld's suggestion implies invariance of the physics along the curves of constant excess entropy in the phase diagram. He validated this using that time's fairly primitive computer simulations of the Lennard-Jones system and a few other simple liquids [29]. Rosenfeld's insight is now referred to as "excess-entropy scaling," a property that has received increasing attention since the turn of the century because it has been found to apply also for many nonsimple systems like liquid mixtures, molecular liquids, confined liquids, crystalline solids, etc. [30].

*dyre@ruc.dk
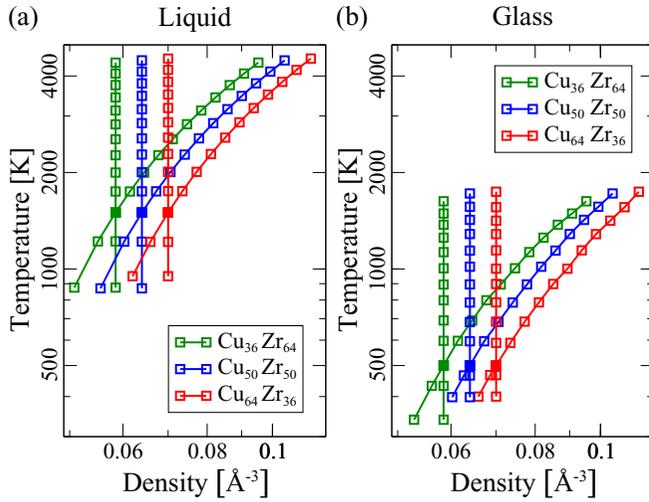
FIG. 1. Logarithmic density-temperature phase diagrams showing all state points simulated along isochores (vertical lines) and isomorphs (lines at an angle). The colors reflect the three different compositions studied. (a) gives liquid state points and (b) gives glass state points. Each isomorph is generated by means of the direct-isomorph-check method (see the text), proceeding in steps of 5% density changes starting from "reference" state points at a temperature of 1500 K for the liquids and 500 K for the glasses (solid symbols). The reference state point densities were selected to have approximately the same pressure ($\sim$ 17 GPa), while the lowest-density state points have approximately zero pressure (compare Tables II and III). The isochores studied for comparison to the isomorphs are the vertical lines through each reference state point.

In the last 20 years, glass science has progressed significantly by the introduction of density scaling, also called thermodynamic scaling. This is the discovery that in the search for a simple mathematical description, the relevant thermodynamic variables are not temperature and pressure, but temperature T and the particle number density ρ [31–36]. When density scaling is applied to experimental data, if γ is the so-called density-scaling exponent, plotting data for the dynamics as a function of ρ^γ/T results in a collapse [32,33,35,36]. This means that the dynamics depends on the two variables of the thermodynamic phase diagram only via the single number ρ^γ/T. It should be emphasized that density scaling is not universally applicable; for instance, it works better for van der Waals liquids and metals than for hydrogen-bonded liquids [33,36,37]. An important extension of density scaling was the discovery of isochronal superposition, according to which not only is the average relaxation time invariant along the curves of constant ρ^γ/T, but so are the frequency-dependent response functions [38–40]. This suggests that the way atoms or molecules move about each other is identical at state points with the same value of ρ^γ/T. One
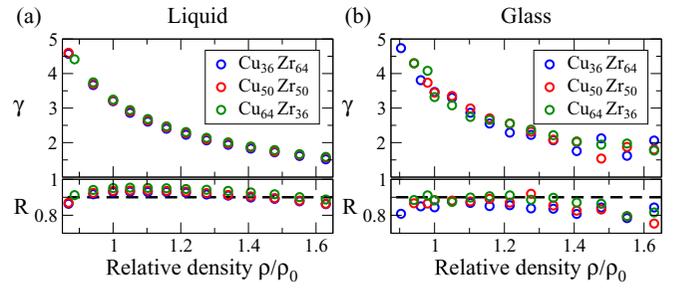
FIG. 2. Virial potential-energy correlation coefficient R [Eq. (5)] and density-scaling exponent γ [Eq. (6)], plotted along the isomorphs as a function of the density relative to that of the reference state point (which has temperature 1500 K for the liquids and 500 K for the glasses). (a) is the liquid and (b) is the glass. We see similar pictures in the two cases, with γ decreasing significantly as density is increased, indicating an effective softening of the interactions. The virial potential-energy correlations are generally strong, with a maximum at densities close to the reference state point densities denoted by ρ_0. The dashed lines mark $R = 0.9$, which is traditionally used for delimiting state points for which isomorph theory predictions are expected to apply [42,59].

may think of this as a "same-movie" property: Filming the atoms/molecules at two such state points results in the same movie except for a uniform scaling of all particle positions and of the time.

The above-mentioned findings can all be derived from the hidden-scale-invariance property stating that the ordering of a system's configurations $\boldsymbol{R} \equiv (\boldsymbol{r}_1, \ldots, \boldsymbol{r}_N)$ (in which N is the number of particles and $\boldsymbol{r}_i$ is the position of particle i) according to their potential energy $U(\boldsymbol{R})$ at one density is maintained if the configurations are scaled uniformly to a different density [41]. The formal mathematical definition of hidden scale invariance is the following logical implication:

$$U(\mathbf{R}_\mathrm{a}) < U(\mathbf{R}_\mathrm{b}) \;\Rightarrow\; U(\lambda\mathbf{R}_\mathrm{a}) < U(\lambda\mathbf{R}_\mathrm{b}). \qquad (1)$$

Equation (1) implies that structure and dynamics, when given in proper reduced units, are invariant along the curves of constant excess entropy, the system's so-called isomorphs [30,41,42]. This result is rigorous if Eq. (1) applies without exception, but that is never the case for realistic models. However, isomorph invariance is still a good approximation if Eq. (1) applies for most of the physically important configurations and for scaling parameters λ relatively close to unity. This is believed to be the case for many metals and van der Waals bonded systems, whereas systems with strong directional bonds like hydrogen-bonded and covalently bonded systems are not expected to obey isomorph theory predictions [43]. For metals the existence of isomorphs has been validated in a few cases [44,45].

TABLE I. EMT parameters for Cu and Zr in CuZr mixtures [57].

Element	s_0 (Å)	E_0 (eV)	λ (Å^{-1})	κ (Å^{-1})	V_0 (eV)	n_0 (Å^{-3})	n_2 (Å^{-1})
Cu	1.41	−3.51	3.693	4.943	1.993	0.0637	3.039
Zr	1.78	−6.30	2.247	3.911	2.32	0.031	2.282

TABLE II. Temperature, density, and pressure of liquid isomorph state points. The bold row represents the reference state point for the isomorph of each composition.

| $Cu_{36}Zr_{64}$ | | | $Cu_{50}Zr_{50}$ | | | $Cu_{64}Zr_{36}$ | | |
T (K)	ρ (Å^{-3})	p (GPa)	T (K)	ρ (Å^{-3})	P (GPa)	T (K)	ρ (Å^{-3})	P (GPa)
875	0.0508	1.7	870	0.0556	0.8	950	0.0620	1.5
1219	0.0551	9.6	1217	0.0602	9.0	1215	0.0659	8.4
1500	**0.0585**	**17.2**	**1500**	**0.0640**	**17.2**	**1500**	**0.0700**	**17.1**
1745	0.0614	24.6	1747	0.0672	25.2	1749	0.0735	25.6
1999	0.0645	33.2	2005	0.0706	34.5	2009	0.0772	35.7
2266	0.0677	43.2	2274	0.0741	45.4	2283	0.0810	47.6
2540	0.0711	54.8	2555	0.0778	58.0	2568	0.0851	61.3
2828	0.0747	68.0	2850	0.0817	72.5	2867	0.0893	77.3
3122	0.0784	83.0	3151	0.0858	89.2	3177	0.0938	95.6
3428	0.0823	100.1	3464	0.0901	108.1	3499	0.0985	116.6
3746	0.0864	119.5	3795	0.0946	129.7	3834	0.1034	140.7
4070	0.0908	141.3	4128	0.0993	154.2	4179	0.1086	168.0
4404	0.0953	165.8	4473	0.1042	181.8	4533	0.1140	199.0

In isomorph theory the density-scaling exponent γ is generally state point dependent. This was recently confirmed in high-pressure experimental data [46–48]. Systems with hidden scale invariance are referred to as R-simple in order to indicate the simplification of the physics that follows from this symmetry; most, but not all, pair-potential systems are R-simple, and several molecular systems are also R-simple, necessitating a specific name for this class of systems.

The purpose of the present paper is to check for isomorphs in a typical metallic glass former. For this we have chosen to study three different CuZr mixtures. As a representative of the Cu-rich alloys that have been most commonly studied in experiments [4–6], we have chosen the 64:36 composition. Supplementing this, we also simulated the 50:50 and the 36:64 compositions. The findings of all three systems are similar. The systems have been computer simulated in both the liquid and glass phases, using the effective-medium theory (EMT)

interaction potentials [49–51]. We find good isomorph invariance of structure and dynamics involving density changes up to a factor of 2. This implies a significant simplification in the description of the physics of this metallic glass former since the thermodynamic phase diagram of CuZr is effectively one-dimensional.

II. THE EFFECTIVE-MEDIUM THEORY POTENTIAL

The EMT potentials [49–51] is one of several similar potentials aimed at describing metals with an accuracy comparable to that of a full density functional theory (DFT) treatment, but at a much lower computational cost. A widely used class of potentials in this group of mean-field potentials is the embedded atom method (EAM) [52,53]. EMT and EAM both write the total energy E as a pair-potential term plus a function of the local electron density at each particle. The EMT realizes this in a semiempirical way, whereas the
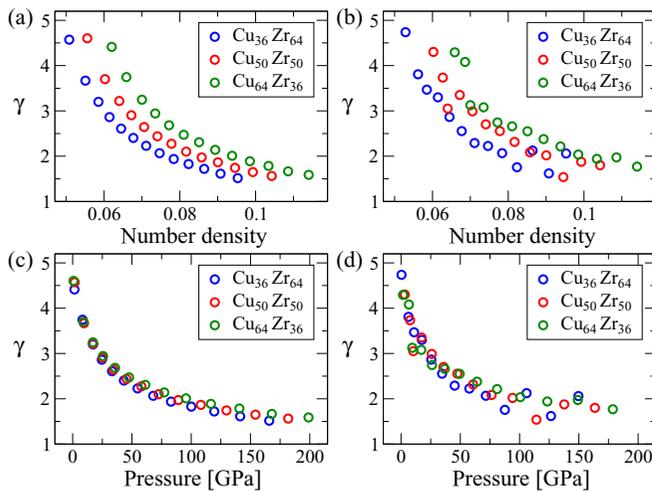
FIG. 3. The density-scaling exponent γ for all state points studied. (a) and (b) show data for γ as a function of the density for the liquid and glass state points, respectively, and (c) and (d) similarly show γ as a function of the pressure.
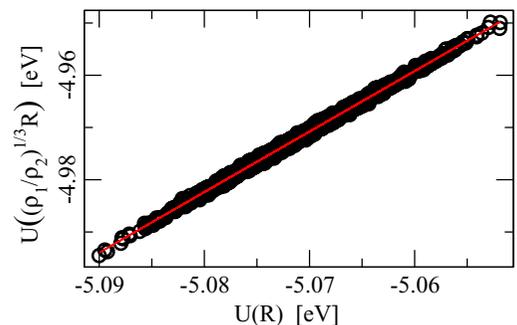
FIG. 4. Example of a direct isomorph check, here with state point 1 being the reference state point of the 64:36 mixture ($T = 1500$ K) and state point 2 having a 5% higher density. At state point 1, a series of thermal-equilibrium configurations $\boldsymbol{R}$ are sampled. Each of these is scaled uniformly by the factor $(\rho_2/\rho_1)^{-1/3} = 0.9839$, resulting in a 5% higher density. Plotting the potential energies of scaled versus unscaled configurations, the slope of the best-fit line is T_2/T_1 [compare Eq. (10)]; this determines the temperature T_2 that makes the state point (ρ_2, T_2) isomorphic to (ρ_1, T_1).

TABLE III. Temperature, density, and pressure of glass isomorph state points. The bold row represents the reference state point for the isomorph of each composition. The starting point for the glass isomorph has the same density as that of the liquid isomorph but the temperature 500 K.

$Cu_{36}Zr_{64}$			$Cu_{50}Zr_{50}$			$Cu_{64}Zr_{36}$		
T (K)	ρ (Å^{-3})	p (GPa)	T (K)	ρ (Å^{-3})	P (GPa)	T (K)	ρ (Å^{-3})	P (GPa)
339	0.0529	0.4	398	0.0602	3.1	400	0.0659	1.7
432	0.0562	6.2	466	0.0627	7.7	467	0.0686	6.6
500	**0.0585**	**11.0**	**500**	**0.0640**	**10.3**	**500**	**0.0700**	**9.5**
587	0.0614	17.6	575	0.0672	17.3	578	0.0735	17.1
683	0.0645	25.5	672	0.0706	25.9	667	0.0772	26.1
781	0.0677	34.6	773	0.0741	35.8	758	0.0810	36.8
880	0.0711	45.2	877	0.0778	47.5	858	0.0851	49.4
980	0.0747	57.6	989	0.0817	60.7	968	0.0893	64.1
1088	0.0784	71.5	1103	0.0858	76.4	1083	0.0938	81.0
1200	0.0823	87.6	1218	0.0901	94.1	1203	0.0985	100.6
1304	0.0864	105.9	1340	0.0946	114.3	1325	0.1034	123.4
1442	0.0908	126.5	1440	0.0993	137.7	1453	0.1086	149.1
1558	0.0953	149.7	1575	0.1042	163.5	1596	0.1140	178.7

parameters of the EAM are determined by fitting to experimental properties of the bulk solid. For more on the relation between the EAM and EMT potentials, the reader is referred to Refs. [49,50], while Ref. [51] gives a detailed derivation of the EMT potential and its parameters. A great advantage of the EMT is that the mathematical expression for the energy is relatively simple. This made it straightforward to implement EMT in our graphics processing unit (GPU) code RUMD [54], whereas the EAM typically involves tabulated data that are not easily implemented efficiently in GPU computing.

The core of the EMT potential is a well-chosen reference system defining the *effective medium*. The total energy of the system is the energy of the reference system plus the difference to the real system. Thus, the EMT total energy is written as

$$E = \sum_i E_{c,i} + \left(E - \sum_i E_{c,i} \right), \quad (2)$$

where $E_{c,i}$ is the so-called cohesive energy, which is the energy of atom i in the reference system. The idea is now that the difference term should be small enough to be treated accurately by first-order perturbation theory. To obtain this

term the reference system must be as close as possible to the real system.

The real and the reference systems are linked by a "tuning parameter." In the first version of the EMT potential, the homogeneous electron gas was used as the reference system, with the electron density as the tuning parameter [55,56]. The EMT version used in the present paper is that of Ref. [51], for which a perfect fcc crystal is the reference system. Here, the lattice constant serves as the tuning parameter, i.e., is used to adjust the environment of an atom such that the average electron density surrounding the atom matches that of the real system.

The EMT potential of a pure metal involves the following parameters: the negative cohesive energy E_0, a charge density parameter n_0, the Wigner-Seitz radius s_0 (defined in terms of the atomic, not the electronic, density), a parameter η quantifying the influence of the density tail surrounding a neighboring atom, a parameter λ determined from the bulk modulus, and finally a quantity determined from the shear modulus. The density-related parameters n_0 and η were originally calculated self-consistently with reference to the homogeneous electron gas, while the five other parameters were determined from experimental or *ab initio* data. More details on how the parameters are determined for single and
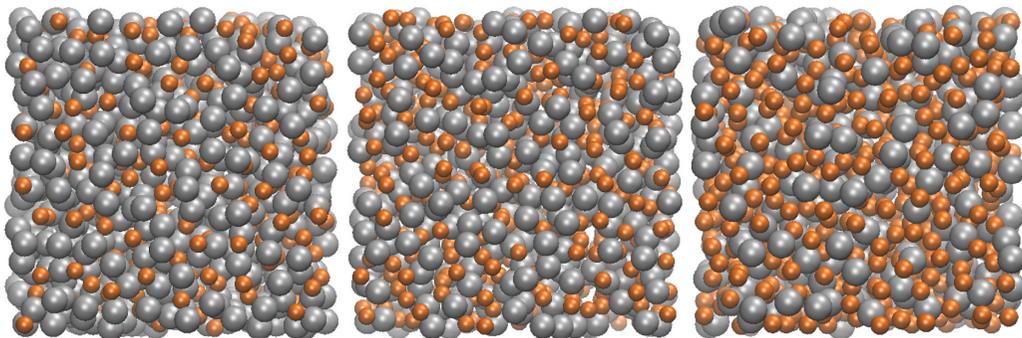
FIG. 5. Snapshots of configurations at the glass isomorph reference state points at 500 K. The Cu atoms are orange; the Zr atoms are gray. From left the snapshots are for the 36:64, 50:50, and 64:36 CuZr compositions.
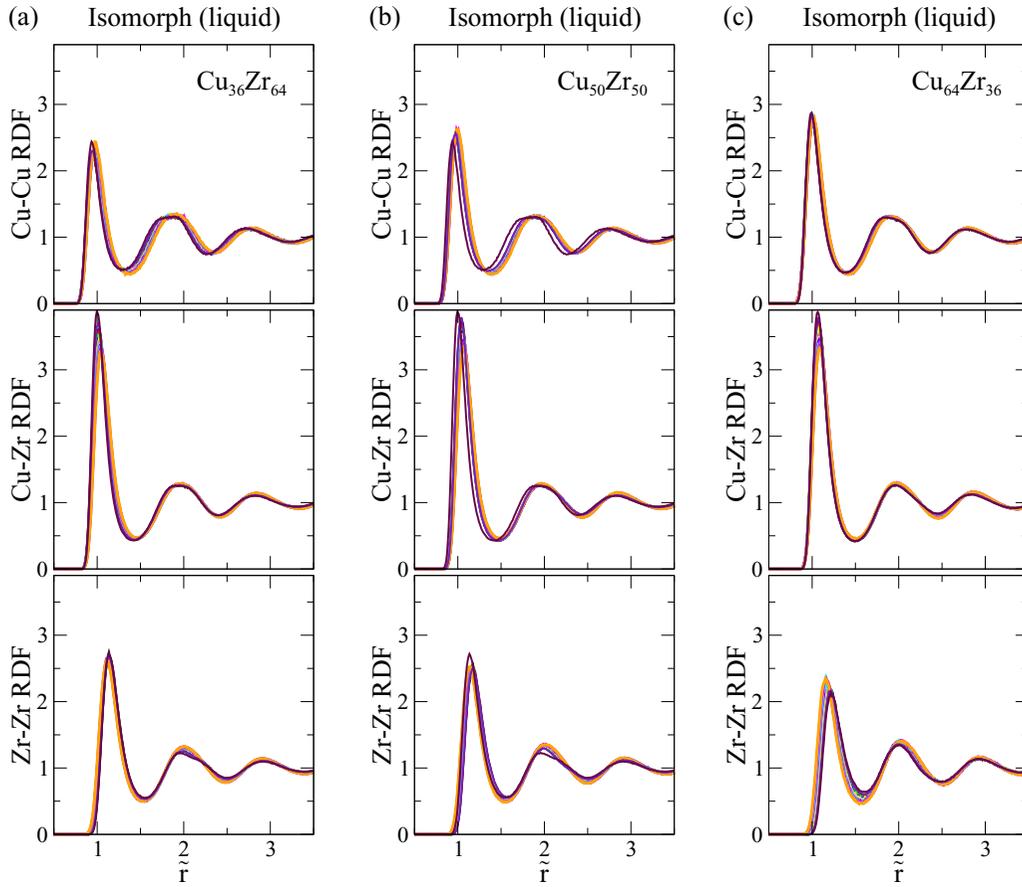
FIG. 6. Liquid-state radial distribution functions (RDFs) plotted as a function of the reduced pair distance $\tilde{r} \equiv \rho^{1/3} r$. (a), (b), and (c) give reduced-unit RDFs along an isomorph for each of the compositions studied. The color coding used is the XMGRACE default ordering, with black for the data set corresponding to the reference state point, then, at increasing density, red, green, blue, yellow, etc.; orange is the color given to the 11th data set, representing the highest temperature. The two state points with lower density than that of the reference state point are purple and brown. Generally, we see approximate isomorph invariance, with some deviation at the first peak maximum and the largest deviations at the lowest densities (at which the virial potential-energy correlation coefficient drops significantly; compare Fig. 2).

compound systems can be found in Refs. [55,57,58]. The parameter values for CuZr used in this work (Table I) are those of Ref. [57], where parameters were adjusted to match DFT-determined cohesive energies, lattice constants, and elastic constants of both the pure metals and a $Cu_{50}Zr_{50}$ alloy.

III. ISOMORPH THEORY

A. Reduced quantities

Structure and dynamics are invariant along isomorphs only when they are given in a "macroscopic" unit system that depends on the state point in question. The unit system defining reduced variables reflects the system's volume V and temperature T as follows. If the particle number density is $\rho \equiv N/V$, the length, energy, and time units are, respectively [42],

$$l_0 = \rho^{-1/3}, \ e_0 = k_B T, \ t_0 = \rho^{-1/3}\sqrt{\frac{m}{k_B T}}. \quad (3)$$

Here m is the average particle mass. Equation (3) refers to Newtonian dynamics; for Brownian dynamics one uses the same length and energy units but a different time unit [42]. All physical quantities can be made dimensionless by reference to

the above units. "Reduced" quantities are denoted by a tilde, for instance,

$$\tilde{\boldsymbol{R}} \equiv \rho^{1/3} \boldsymbol{R}. \quad (4)$$

B. Tracing out isomorphic state points

Three compositions were studied, $Cu_{36}Zr_{64}$, $Cu_{50}Zr_{50}$, and $Cu_{64}Zr_{36}$. Figure 1 presents the state points simulated in a density-temperature thermodynamic phase diagram. Isomorph invariance is never perfect in realistic systems. In order to estimate to what degree this invariance holds, it is therefore useful to compare structure and dynamics variations along isomorphs to what happens along curves of similar temperature or density variation which are not isomorphs. We have chosen to make a comparison to isochores (lines of constant density) with the same temperature variation as the isomorphs. The isochores studied are the vertical straight lines in Fig. 1; the isomorphs are the lines with a slope. The high-temperature state points describe equilibrium liquids (left); the low-temperature points are glass-phase state points (right).

We now turn to the challenge of tracing out isomorphs. Recall that an isomorph is a curve of constant S_{ex} for a
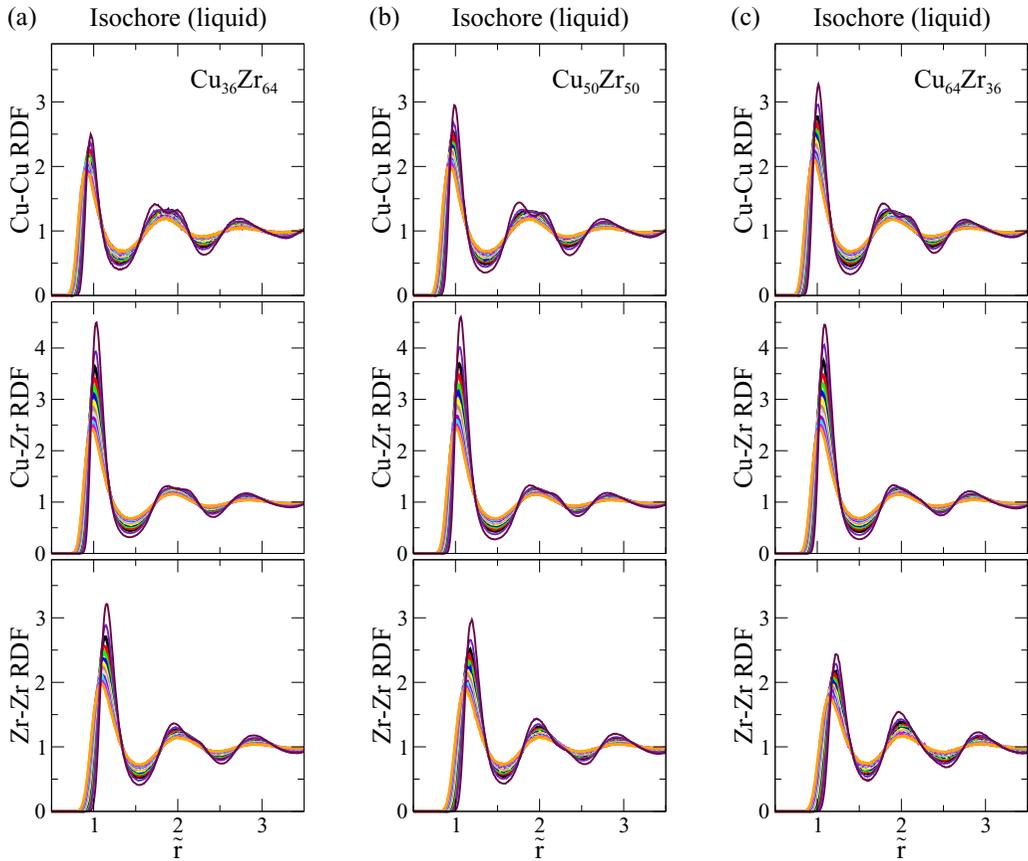
FIG. 7. Liquid-state RDFs along the reference-state-point density isochores plotted as in Fig. 6. There is a considerable variation of the structure, being more washed out the higher the temperature is. This is an effect of the increasing thermal fluctuations.

system that obeys the hidden-scale-invariance condition (1) at the relevant state points. To which degree this condition is obeyed may be difficult to judge because Eq. (1) always applies when λ is close to unity, but fortunately, a practical criterion exists: Eq. (1) applies to a good approximation if and only if the virial W and potential energy U are strongly cor-

related in their thermal-equilibrium constant-density (NVT) fluctuations [41]. These fluctuations are characterized by the Pearson correlation coefficient R defined by

$$R = \frac{\langle \Delta U \, \Delta W \rangle}{\sqrt{\langle (\Delta U)^2 \rangle \langle (\Delta W)^2 \rangle}} , \tag{5}$$
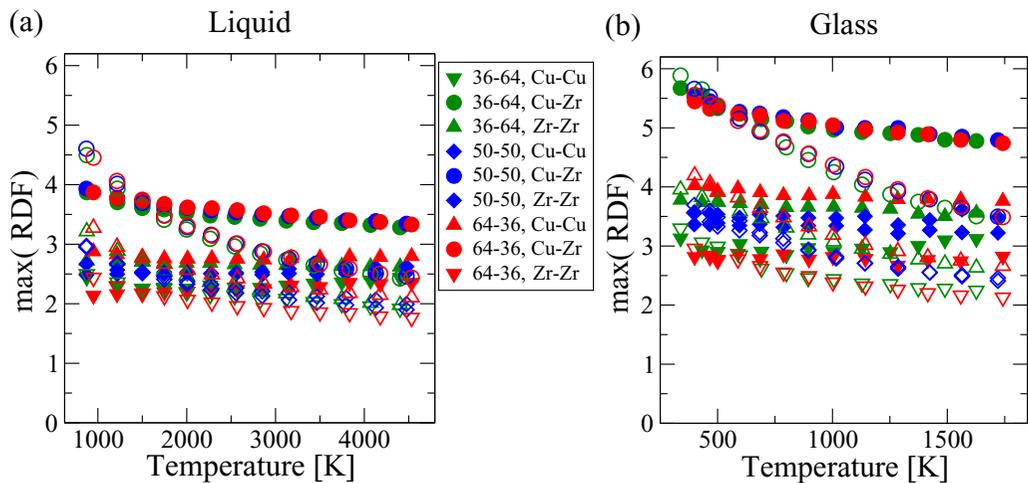
FIG. 8. Maximum values of all RDFs of Figs. 6 and 7, i.e., the RDF values at their first peak, with (a) showing results for the liquids and (b) showing results for the glasses. The solid symbols represent isomorph data; the open symbols represent isochore data. While the isomorph values are not invariant, in particular for the Cu-Zr RDFs, for both liquids and glasses the general picture is that of a significantly better invariance along the isomorphs than along the isochores.
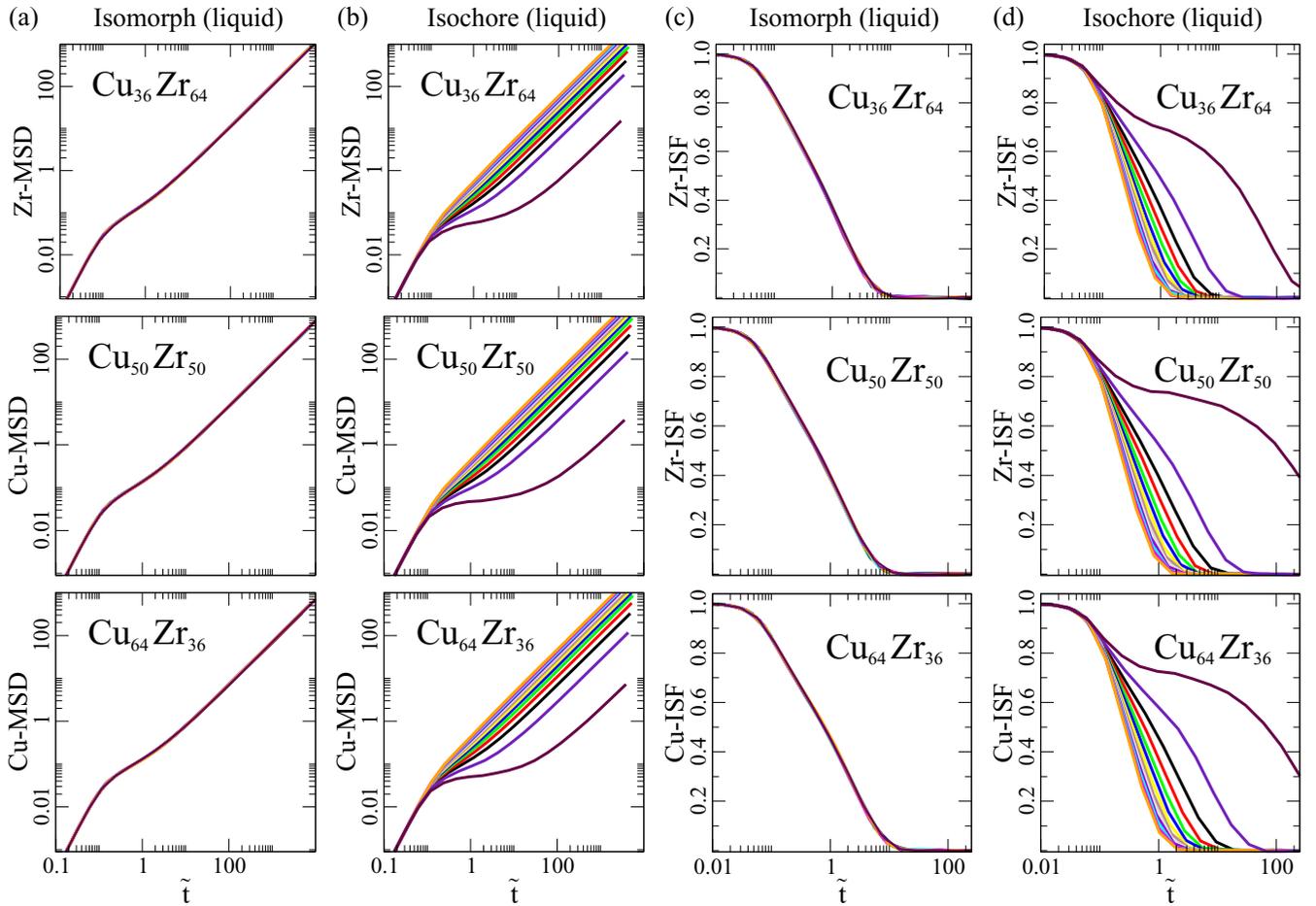
FIG. 9. Dynamics along the isomorphs and isochores of the liquids. (a) and (b) give data for the reduced mean-square displacement (MSD) as a function of the reduced time; (c) and (d) give the reduced intermediate incoherent scattering function (ISF) at the wave vector $2\pi\rho^{1/3}$ (which is constant in reduced units). There is good isomorph invariance of the dynamics but a significant variation along the isochores (except in the short-time ballistic region where the reduced MSD by definition is $3\tilde{t}^2$ at all state points).

where angle brackets denote canonical-ensemble averages and Δ is the deviation from the thermal average. As a pragmatic criterion, $R > 0.9$ is usually used for delimiting where isomorph theory predictions are expected to apply [42,43,59]. For the CuZr systems we find that R goes below 0.9 at high densities in the liquid phase, as well as in most of the glass phase (Fig. 2), but at most state points studied R is above 0.8. Thus, it makes good sense to test for isomorph invariance.

Tracing out a curve of constant excess entropy is straightforward if one knows how S_{ex} varies throughout the phase diagram. It is a bit challenging to evaluate entropy, however, because doing so involves thermodynamic integration (or the Widom insertion method, which is also tedious). In order to trace out an isomorph, one does not need to know the value of S_{ex}, however, and can instead make use of the following identity:

$$\gamma \equiv \left(\frac{\partial \ln T}{\partial \ln \rho}\right)_{S_{ex}} = \frac{\langle \Delta U \Delta W \rangle}{\langle (\Delta U)^2 \rangle}. \tag{6}$$

Here, the quantity γ is the (state-point-dependent) density-scaling exponent defined as the isomorph slope in a logarithmic density-temperature phase diagram like those in Fig. 1.

The second equality sign is a statistical-mechanical identity that allows for calculating γ from NVT equilibrium fluctuations at the state point in question [42]. Figure 2 shows how γ varies along the isomorphs of the CuZr systems studied below, plotted as a function of the density relative to that of the isomorph reference state point. All cases show similar behavior, with γ decreasing significantly with increasing density. This indicates a softening of the interactions at high densities.

Figure 3 looks more closely into what controls the density-scaling exponent γ. Figures 3(a) and 3(b) show γ as a function of the (number) density for, respectively, the liquid and glass state points. While there is a good collapse when γ is plotted as a function of density relative to the reference-state-point density (Fig. 2), that is no longer the case. Interestingly, plotting γ as a function of the pressure results in an approximate data collapse [Figs. 3(c) and 3(d)]. This finding is consistent with a recent conjecture by Casalini and Ransom that was formulated in the entirely different context of supercooled organic liquids [48]. The glass data are more noisy than the liquid data, which we ascribe to the fact that a glass consists of atoms vibrating in a single potential-energy minimum; that is, just a single so-called inherent state is monitored.
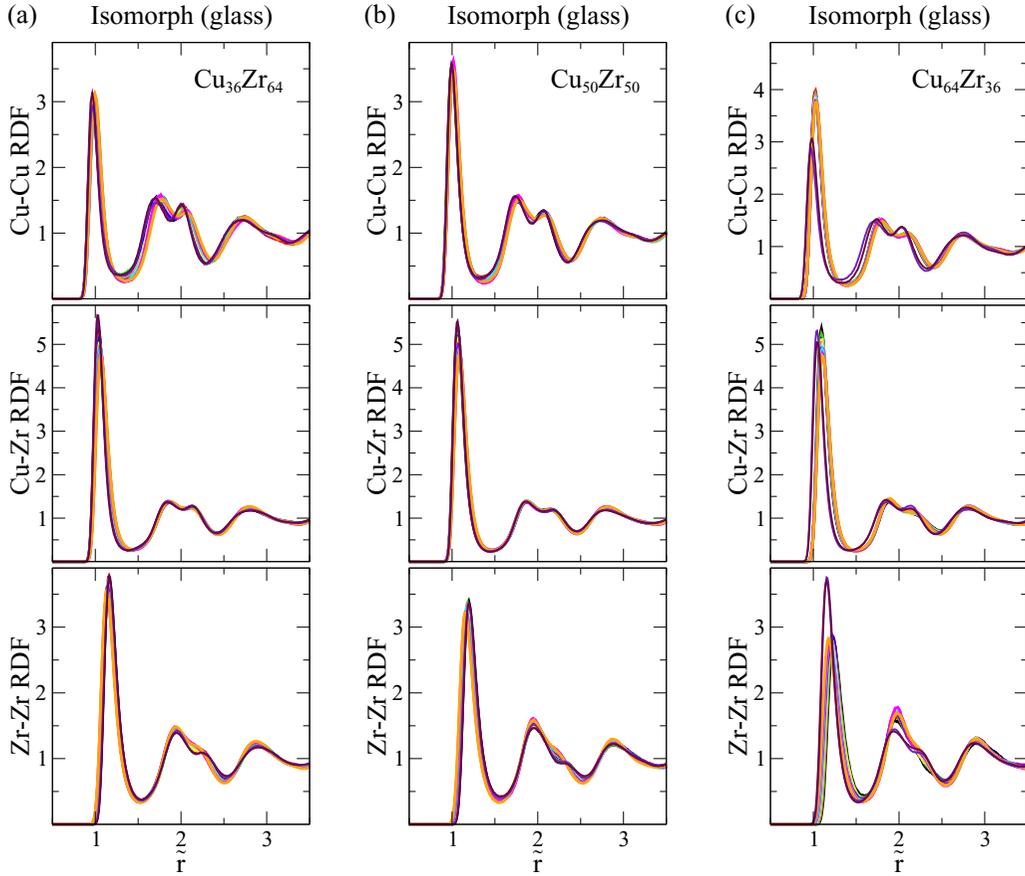
FIG. 10. Glass-state RDFs plotted as a function of the reduced pair distance $\tilde{r}$. (a), (b), and (c) give reduced-unit RDFs along an isomorph for each of the compositions studied. The picture is pretty much the same as in the liquid phase, except for the somewhat more noisy data that reflect the fact that, basically, only a single configuration and its vibrations are probed. Significant deviations from isomorph invariance are observed for the 64% Cu mixture, both at the highest densities for the Cu-Cu RDF and at the lowest densities for the Zr-Zr RDF.

Equation (6) can be used to trace out an isomorph by numerical integration, using the Euler algorithm for density changes of the order of 1% [42] or using the fourth-order Runge-Kutta algorithm that allows for significantly larger density changes [60]. While both methods are accurate, they involve many simulations if one wishes to cover a significant density range. Fortunately, there are computationally more efficient methods. For instance, isomorphs of the Lennard-Jones system are, to a good approximation, given by $h(\rho)/T = \text{const}$, where $h(\rho) = (\gamma_0/2 - 1)(\rho/\rho_0)^4 - (\gamma_0/2 - 2)(\rho/\rho_0)^2$, in which γ_0 is the density-scaling exponent at a selected reference state point of density ρ_0 [61,62].

A general and efficient method for tracing out isomorphs is the "direct isomorph check" (DIC) [42], which we used to generate the CuZr isomorphs. The DIC is justified as follows [41]. Hidden scale invariance [Eq. (1)] implies that the microscopic excess entropy function $S_{ex}(\boldsymbol{R})$ is scale invariant, i.e., a function only of a configuration's reduced coordinate $\tilde{\boldsymbol{R}}$: $S_{ex}(\boldsymbol{R}) = S_{ex}(\tilde{\boldsymbol{R}})$ [41]. From the definition of $S_{ex}(\boldsymbol{R})$ it follows that $U(\boldsymbol{R}) = U(\rho, S_{ex}(\tilde{\boldsymbol{R}}))$, where the function $U(\rho, S_{ex})$ is the average potential energy at the state point with density ρ and excess entropy S_{ex} [41]. Considering configurations with the same density ρ and small deviations in the microscopic excess entropy from that of the given state point S_{ex}, an ex-

pansion to first order leads to

$$U(\boldsymbol{R}) \cong U(\rho, S_{ex}) + T(\rho, S_{ex})[S_{ex}(\tilde{\boldsymbol{R}}) - S_{ex}]. \quad (7)$$

Consider two state points, (ρ_1, T_1) and (ρ_2, T_2), with the same excess entropy S_{ex} and with average potential energies U_1 and U_2, respectively. If $\boldsymbol{R}_1$ and $\boldsymbol{R}_2$ are configurations of these state points with the same reduced coordinates, i.e., obeying

$$\rho_1^{1/3}\boldsymbol{R}_1 = \rho_2^{1/3}\boldsymbol{R}_2 \equiv \tilde{\boldsymbol{R}}, \quad (8)$$

one gets, by elimination of the common factor $S_{ex}(\tilde{\boldsymbol{R}}) - S_{ex}$ in Eq. (7) with $T_1 \equiv T(\rho_1, S_{ex})$ and $T_2 \equiv T(\rho_2, S_{ex})$,

$$\frac{U(\boldsymbol{R}_1) - U_1}{T_1} \cong \frac{U(\boldsymbol{R}_2) - U_2}{T_2}. \quad (9)$$

While not of direct relevance for the present paper, we note that Eq. (9) implies $\exp[-U(\boldsymbol{R}_1)/k_B T_1] \propto \exp[-U(\boldsymbol{R}_2)/k_B T_2]$, implying that the two configurations have the same canonical probability.

Equation (9) leads to $U(\boldsymbol{R}_2) \cong (T_2/T_1)U(\boldsymbol{R}_1) + [U_2 - (T_2/T_1)U_1]$. For the fluctuations about the respective mean values this implies

$$\Delta U(\boldsymbol{R}_2) \cong \frac{T_2}{T_1}\Delta U(\boldsymbol{R}_1). \quad (10)$$
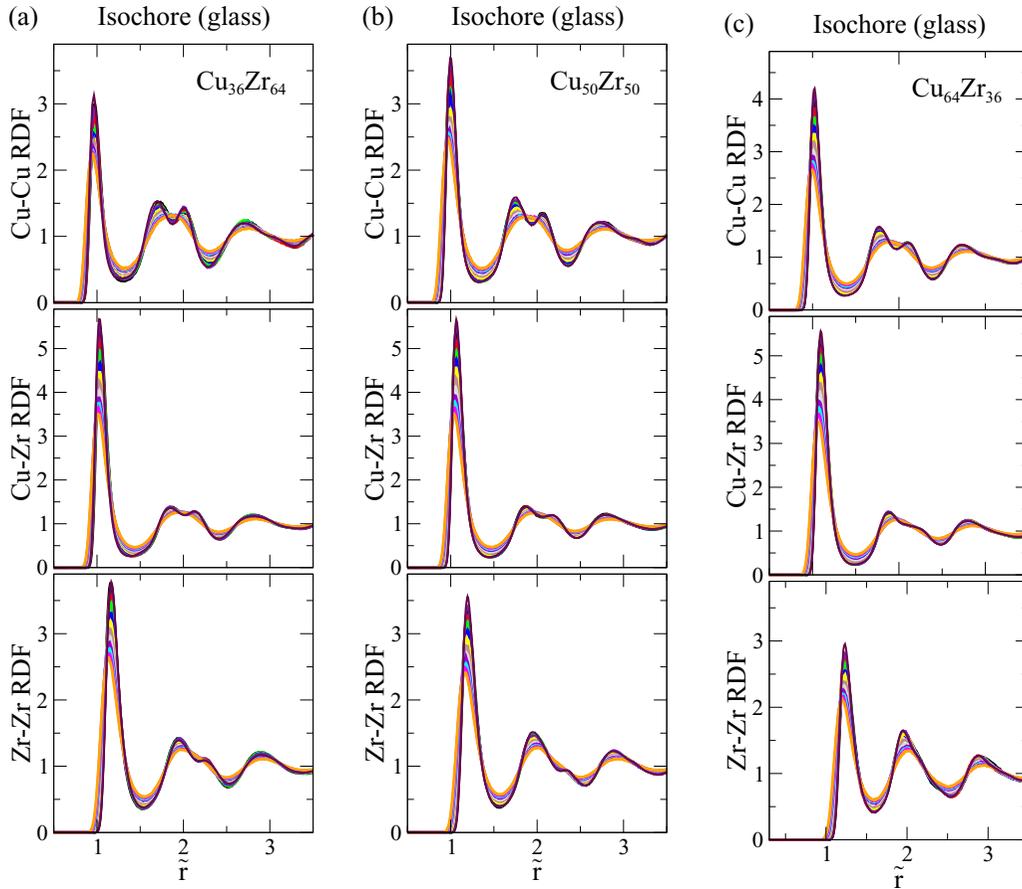
FIG. 11. Glass-state RDFs along the reference-state-point isochores plotted as in Fig. 10, showing a considerably larger variation.

Equation (10) implies that isomorphic state points may be identified as follows: First, sample a set of equilibrium configurations at state point (ρ_1, T_1). Then scale these configurations uniformly to density ρ_2. The temperature T_2 of the state point with density ρ_2, which is isomorphic to the state point (ρ_1, T_1), is now found from the slope of a scatter plot of the potential energies of scaled versus unscaled configurations. An example of how this works is shown in Fig. 4.

Because the hidden-scale-invariance property is not exact, the DIC is less reliable for large density changes than for smaller ones. We traced out the isomorphs studied below using step-by-step DICs involving density changes of 5%. The resulting isomorphs are shown in Fig. 1. The simulated isomorphic state points are listed in Table II (liquid) and Table III (glass).

IV. SIMULATION DETAILS

The three compositions studied in this work are Cu_xZr_{100-x} ($x = 36, 50, 64$). For each of these an isomorph was generated from a state point well into the liquid regime. From this initial "reference" state point at temperature 1500 K, an isomorph was traced out using the DIC as described above. The majority of state points are at a higher density than that of the reference state point ρ_0, but for each isomorph we also generated two isomorph state points at lower densities to ensure that samples

close to zero pressure were included in the study (compare Tables II and III).

The NVT ensemble implemented via the standard Nosé-Hoover thermostat was used to simulate cubic boxes containing 1000 particles. For each state point on an isomorph, a state point was simulated at the same temperature at the reference-state-point density; these constitute the isochoric state points discussed below along with the isomorph state points. The glass-phase reference state points were obtained by cooling at a constant rate in 100 000 time steps from the liquid reference state point at 1500 K to the glass isomorph reference temperature 500 K. The cooling was implemented by adjusting the Nosé-Hoover temperature in each step. Since a time step corresponds to 5.1 fs, this cooling rate corresponds roughly to 2 K/ps. From the three glass reference state points, isomorphs were generated by the DIC method in the same way as for the liquids.

The simulations were carried out in RUMD [54], Roskilde University's GPU molecular dynamics package that is optimized for small systems. At each state point the initial configuration was a simple cubic crystal with particle types assigned randomly at the required ratios. At each state point of the liquid, 10^4 molecular dynamics (MD) steps of equilibration were performed to melt and equilibrate the liquid. Afterward, we carried out 10^6 MD steps for each production run. For the glass-phase simulations, 10^5 MD steps of equilibration were performed before 10^7 MD steps of the production
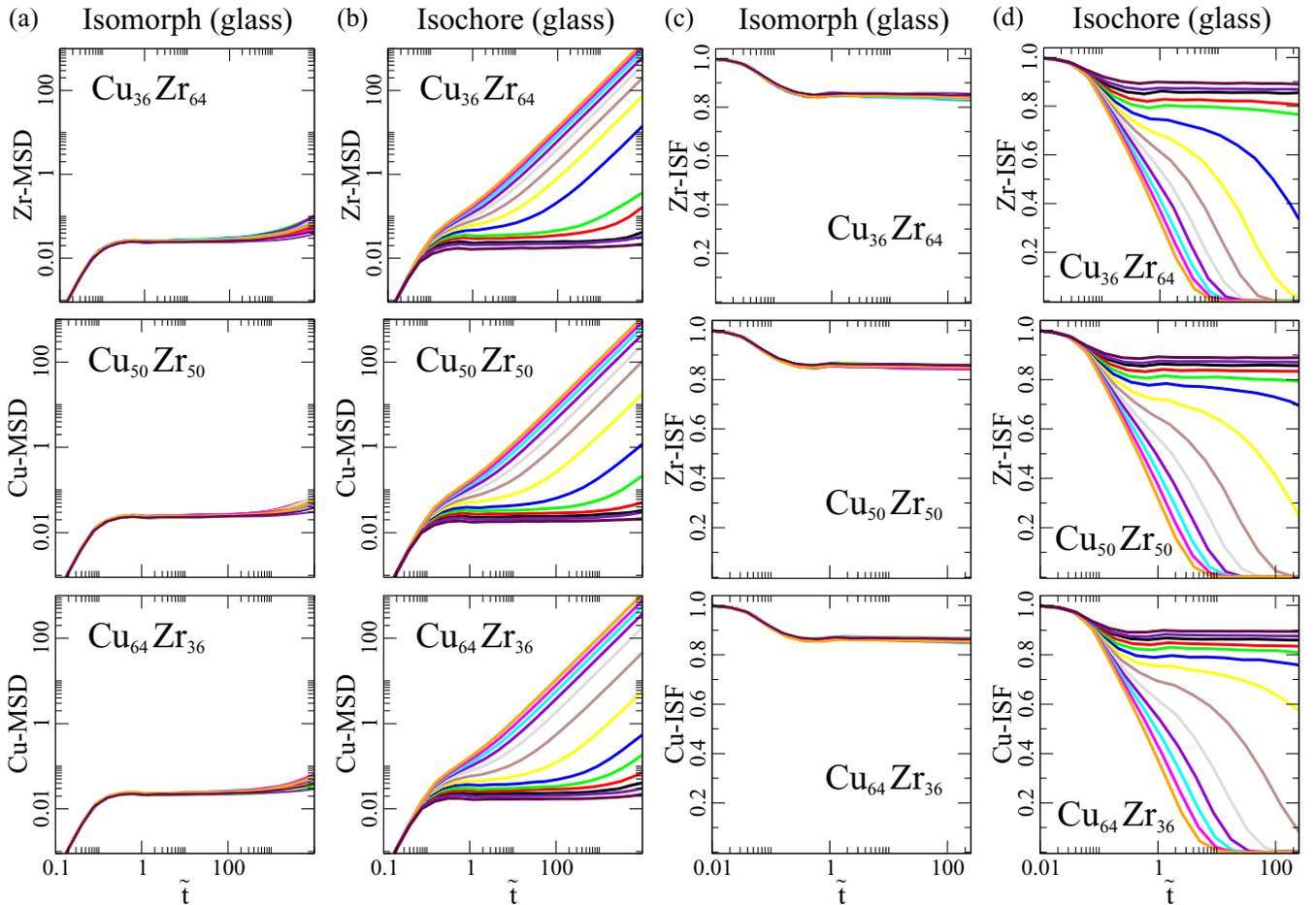
FIG. 12. Dynamics along the glass isomorphs and isochores. (a) and (b) give data for the reduced MSD as a function of the reduced time; (c) and (d) give the reduced-unit intermediate incoherent scattering function at the wave vector $2\pi\rho^{1/3}$. Because the system is a glass, along the isomorphs the MSD is constant over a very long time, and correspondingly, the incoherent intermediate scattering function does not decay to zero. For the isochore state points, raising the temperature takes the system closer to a liquid with a MSD that at long times is proportional to time and an intermediate incoherent scattering function that decays to zero at long times. The overall picture is that, as for the liquids (Fig. 9), there is good isomorph invariance of the dynamics but a significant variation along the isochores.

run. The time step in the simulations was $0.5\,\text{Å}^{1/2}\,(\text{u/eV})^{1/2}$, where u is the atomic mass unit.

Figure 5 shows the glasses prepared by cooling the liquids to the glass isomorph reference state points. There are no signs of crystallization.

V. STRUCTURE AND DYNAMICS IN THE LIQUID PHASE

To investigate how the structure varies along isomorphs and isochores for the three CuZr compositions we probed the RDFs, which in reduced units are predicted to be isomorph invariant. There are three different RDFs, one for Cu-Cu, one for Cu-Zr, and one for Zr-Zr. Plotting a RDF in reduced units implies scaling the distance variable according to the density [compare Eq. (4)]. This results in peaks at roughly the same places for all compositions because the scaling corresponds to taking the system to unit density.

Figure 6 shows the reduced RDFs along the isomorphs, and Fig. 7 shows similar RDFs along isochores with the same temperature variation (compare to Fig. 1, showing the simulated state points). Comparing the two, we conclude that the

structure is isomorph invariant to a good approximation but varies significantly along the isochores. Deviations are largest for the minority-minority RDFs of the two nonequimolar compositions. Deviations from isomorph invariance are also seen in some cases at the first maximum, where the maximum is generally lowered somewhat with increasing density. This is an effect that is well understood for pair-particle systems, for which it derives from the fact that a higher density-scaling exponent γ implies a steeper effective pair potential and therefore less likely particle close encounters. This decrease of the probability of near encounters results in moving some of the low-distance RDFs to higher distances when γ is large, which is the case at low densities. This explanation suggests that γ of the present non-pair-potential simulations can also be interpreted as an effective inverse-power-law (IPL) pair-potential exponent [44]. For the isochores, there is a general "damping" of the RDFs at all distances as temperature increases. This reflects the stronger thermal fluctuations at high temperatures.

Focusing on the height of the first RDF peak, Fig. 8 shows the peak heights for all the data of Figs. 6 and 7; for ease of comparison we included here also the analogous data for

the glass-phase simulations (Sec. VI). The solid symbols are the peak heights along the three isomorphs, whereas the open symbols are the peak heights along the corresponding isochores. Clearly, the variation is significantly larger along the isochores.

Next, we investigated the liquid-phase dynamics. Figures 9(a) and 9(b) show results for the reduced-unit mean-square displacement (MSD) along isomorphs and isochores, respectively. We focus on the majority-atom MSD but found that data for the minority atom are entirely similar (not shown). Clearly, the MSD is isomorph invariant and varies significantly along the isochores. Note that the short-time ballistic-region collapse seen in all cases follows from the definition of reduced units; that is, this collapse applies throughout the phase diagram of any system. Figures 9(c) and 9(d) show similar data for the incoherent intermediate scattering function evaluated at the wave vector $2\pi\rho^{1/3}$ (which is constant in reduced units). Again, isomorph invariance is clearly demonstrated.

Returning to Fig. 8, in view of Fig. 9, one may ask, Which structural features are most important for the dynamics? Figure 8 shows that the majority-component self-RDF shows the best isomorphic scaling. This suggests that the dynamics of all atoms are largely determined by the majority species, i.e., that the two nonequimolar mixtures act as effective one-component systems.

VI. STRUCTURE AND DYNAMICS IN THE GLASS PHASE

The above investigation was repeated in the glass phase of the three mixtures. Isomorph theory is traditionally formulated with reference to thermal equilibrium [41–43], but we ignored this and proceeded pragmatically as if a glass were an equilibrium system. Each of the three glasses was prepared by cooling with a constant rate from a configuration at the reference state point ($T = 1500\,\text{K}$) to the temperature 500 K. For each composition, once a glass configuration was obtained at the reference state point, we generated an isomorph in the same way as for the liquid isomorphs by repeated DICs involving 5% density changes. Again, for comparison we also probed the RDF and the dynamics at isochoric state points with the same temperature variation as that of the isomorphs (Fig. 1).

The RDFs are shown in Fig. 10 (isomorphs) and in Fig. 11 (isochores). The picture is similar to that of the liquid phase: Overall, good invariance along the isomorphs is seen, in contrast to a substantially larger variation observed along the isochores. This is also the conclusion from Fig. 8, which shows all the first-peak heights as a function of the temperature.

The dynamics of the glasses is investigated via the MSD and the incoherent intermediate structure factor in Fig. 12. A glass consists mostly of atoms frozen at fixed positions, merely vibrating there. Thus, the MSD is virtually constant,

though some particle motion is discernible at the longest times. This "glass flow" motion does not appear to be isomorph invariant, but we found no systematic variation of it with the density. This indicates that the noninvariance reflects statistical uncertainty. Along the isochores [Fig. 12(b)], it is clear that the glass gradually melts as temperature is increased when heating from the black curve representing the 500 K reference state point. The fact that the particles in the glass virtually do not move except for vibrations is also visible in the incoherent intermediate scattering function [Figs. 12(c) and 12(d)], which along the isomorphs stabilizes at a constant level at long times. In contrast, many of the isochore curves go to zero at long times, reflecting an increased ease of motion with increasing temperature that is not achieved along the isomorphs.

As mentioned, a glass is an out-of-equilibrium system, i.e., not a typical member of a canonical-ensemble distribution. It may be surprising that one can ignore this fact and go ahead by constructing isomorphs using the direct isomorph check, resulting in isomorphs that turn out to work basically just as well as the equilibrium-liquid-state isomorphs in regard to invariance properties. This confirms that even glass configurations obey the hidden-scale-invariance condition (1), which is not limited to equilibrium configurations [63].

VII. SUMMARY

This paper has studied three different compositions of the CuZr system by computer simulations using the computationally efficient EMT potentials. We have traced out isomorphs in the liquid and glass phases of the three systems. Good isomorph invariance was observed for structure and dynamics in both phases, showing that the atoms move about each other in much the same way at state points on the same isomorph. This means that the thermodynamic phase diagram of CuZr systems is effectively one-dimensional. Thus, for many purposes, in order to get an overview of the CuZr system, it is enough to investigate state points belonging to different isomorphs. It should be noted, though, that some quantities like the bulk modulus are not isomorph invariant even when given in reduced units [64]. On the other hand, most material quantities *are* isomorph invariant in reduced units, e.g., the shear modulus, the shear viscosity, the heat conductivity, etc. [64].

It would be interesting to confirm the above results using EAM potentials [37]. Given that the EAM and EMT both have been shown to nicely reproduce metal properties, we do not expect significantly different results. Indeed, that isomorph theory describes metals well has been validated by DFT simulations of crystals [44].

[1] A. L. Greer, Metallic glasses, Science **267**, 1947 (1995).

[2] M. Zink, K. Samwer, W. L. Johnson, and S. G. Mayr, Plastic deformation of metallic glasses: Size of shear transformation

zones from molecular dynamics simulations, Phys. Rev. B **73**, 172203 (2006).

[3] M. I. Mendelev, M. J. Kramer, R. T. Ott, and D. J. Sordelet, Molecular dynamics simulation of diffusion in supercooled Cu-Zr alloys, Philos. Mag. **89**, 109 (2009).

[4] W. H. Wang, The elastic properties, elastic models and elastic perspectives of metallic glasses, Prog. Mater. Sci. **57**, 487 (2012).

[5] W. H. Wang, Dynamic relaxations and relaxation-property relationships in metallic glasses, Prog. Mater. Sci. **106**, 100561 (2019).

[6] M.-B. Tang, D.-Q. Zhao, M.-X. Pan, and W.-H. Wang, Binary Cu-Zr bulk metallic glasses, Chin. Phys. Lett. **21**, 901 (2004).

[7] S. A. Rice and P. Gray, *The Statistical Mechanics of Simple Liquids* (Interscience, New York, 1965).

[8] H. N. V. Temperley, J. S. Rowlinson, and G. S. Rushbrooke, *Physics of Simple Liquids* (Wiley, New York, 1968).

[9] S. M. Stishov, The thermodynamics of melting of simple substances, Sov. Phys. Usp. **17**, 625 (1975).

[10] J.-L. Barrat and J.-P. Hansen, *Basic Concepts for Simple and Complex Liquids* (Cambridge University Press, Cambridge, 2003).

[11] T. S. Ingebrigtsen, T. B. Schrøder, and J. C. Dyre, What Is a Simple Liquid? Phys. Rev. X **2**, 011011 (2012).

[12] J.-P. Hansen and I. R. McDonald, *Theory of Simple Liquids: With Applications to Soft Matter*, 4th ed. (Academic, New York, 2013).

[13] J. O. Hirschfelder, C. F. Curtiss, and R. B. Bird, *Molecular Theory of Gases and Liquids* (Wiley, New York, 1954).

[14] J. D. Bernal, The Bakerian lecture, 1962. The structure of liquids, Proc. R. Soc. London, Ser. A **280**, 299 (1964).

[15] B. Widom, Intermolecular forces and the nature of the liquid state, Science **157**, 375 (1967).

[16] J. A. Barker and D. Henderson, What is "liquid"? Understanding the states of matter, Rev. Mod. Phys. **48**, 587 (1976).

[17] D. Chandler, J. D. Weeks, and H. C. Andersen, Van der Waals picture of liquids, solids, and phase transformations, Science **220**, 787 (1983).

[18] J. C. Dyre, Simple liquids' quasiuniversality and the hard-sphere paradigm, J. Phys.: Condens. Matter **28**, 323001 (2016).

[19] J. D. van der Waals, Over de Continuiteit van den Gas- en Vloeistoftoestand, dissertation, University of Leiden, 1873.

[20] J. S. Rowlinson, The statistical mechanics of systems with steep intermolecular potentials, Mol. Phys. **8**, 107 (1964).

[21] D. Henderson and J. A. Barker, Perturbation theory of fluids at high temperatures, Phys. Rev. A **1**, 1266 (1970).

[22] H. C. Andersen, J. D. Weeks, and D. Chandler, Relationship between the hard-sphere fluid and fluids with realistic repulsive forces, Phys. Rev. A **4**, 1597 (1971).

[23] H. S. Kang, S. C. Lee, T. Ree, and F. H. Ree, A perturbation theory of classical equilibrium fluids, J. Chem. Phys. **82**, 414 (1985).

[24] K. R. Harris, The selfdiffusion coefficient and viscosity of the hard sphere fluid revisited: A comparison with experimental data for xenon, methane, ethene and trichloromethane, Mol. Phys. **77**, 1153 (1992).

[25] J. E. Straub, Analysis of the role of attractive forces in self-diffusion of a simple fluid, Mol. Phys. **76**, 373 (1992).

[26] D. Ben-Amotz and G. Stell, Reformulaton of Weeks–Chandler–Andersen perturbation theory directly in terms of a hard-sphere reference system, J. Phys. Chem. B **108**, 6877 (2004).

[27] A. E. Nasrabad, Thermodynamic and transport properties of the Weeks–Chandler–Andersen fluid: Theory and computer simulation, J. Chem. Phys. **129**, 244508 (2008).

[28] T. Rodriguez-Lopez, J. Moreno-Razo, and F. del Rio, Thermodynamic scaling and corresponding states for the self-diffusion coefficient of non-conformal soft-sphere fluids, J. Chem. Phys. **138**, 114502 (2013).

[29] Y. Rosenfeld, Relation between the transport coefficients and the internal entropy of simple systems, Phys. Rev. A **15**, 2545 (1977).

[30] J. C. Dyre, Perspective: Excess-entropy scaling, J. Chem. Phys. **149**, 210901 (2018).

[31] D. Kivelson, G. Tarjus, X. Zhao, and S. A. Kivelson, Fitting of viscosity: Distinguishing the temperature dependences predicted by various models of supercooled liquids, Phys. Rev. E **53**, 751 (1996).

[32] C. Alba-Simionesco, A. Cailliaux, A. Alegria, and G. Tarjus, Scaling out the density dependence of the alpha relaxation in glass-forming polymers, Europhys. Lett. **68**, 58 (2004).

[33] C. M. Roland, S. Hensel-Bielowka, M. Paluch, and R. Casalini, Supercooled dynamics of glass-forming liquids and polymers under hydrostatic pressure, Rep. Prog. Phys. **68**, 1405 (2005).

[34] D. Gundermann, U. R. Pedersen, T. Hecksher, N. P. Bailey, B. Jakobsen, T. Christensen, N. B. Olsen, T. B. Schrøder, D. Fragiadakis, R. Casalini, C. M. Roland, J. C. Dyre, and K. Niss, Predicting the density–scaling exponent of a glass–forming liquid from Prigogine–Defay ratio measurements, Nat. Phys. **7**, 816 (2011).

[35] E. R. Lopez, A. S. Pensado, J. Fernandez, and K. R. Harris, On the density scaling of pVT data and transport properties for molecular and ionic liquids, J. Chem. Phys. **136**, 214502 (2012).

[36] K. Adrjanowicz, M. Paluch, and J. Pionteck, Isochronal superposition and density scaling of the intermolecular dynamics in glass-forming liquids with varying hydrogen bonding propensity, RSC Adv. **6**, 49370 (2016).

[37] Y.-C. Hu, B.-S. Shang, P.-F. Guan, Y. Yang H.-Y. Bai, and W.-H. Wang, Thermodynamic scaling of glassy dynamics and dynamic heterogeneities in metallic glass-forming liquid, J. Chem. Phys. **145**, 104503 (2016).

[38] C. M. Roland, R. Casalini, and M. Paluch, Isochronal temperature–pressure superpositioning of the alpha–relaxation in type-A glass formers, Chem. Phys. Lett. **367**, 259 (2003).

[39] K. L. Ngai, R. Casalini, S. Capaccioli, M. Paluch, and C. M. Roland, Do theories of the glass transition, in which the structural relaxation time does not define the dispersion of the structural relaxation, need revision? J. Phys. Chem. B **109**, 17356 (2005).

[40] H. W. Hansen, A. Sanz, K. Adrjanowicz, B. Frick, and K. Niss, Evidence of a one-dimensional thermodynamic phase diagram for simple glass-formers, Nat. Commun. **9**, 518 (2018).

[41] T. B. Schrøder and J. C. Dyre, Simplicity of condensed matter at its core: Generic definition of a Roskilde-simple system, J. Chem. Phys. **141**, 204502 (2014).

[42] N. Gnan, T. B. Schrøder, U. R. Pedersen, N. P. Bailey, and J. C. Dyre, Pressure-energy correlations in liquids. IV. "Isomorphs" in liquid phase diagrams, J. Chem. Phys. **131**, 234504 (2009).

[43] J. C. Dyre, Hidden scale invariance in condensed matter, J. Phys. Chem. B **118**, 10007 (2014).

[44] F. Hummel, G. Kresse, J. C. Dyre, and U. R. Pedersen, Hidden scale invariance of metals, Phys. Rev. B **92**, 174116 (2015).

[45] L. Friedeheim, J. C. Dyre, and N. P. Bailey, Hidden scale invariance at high pressures in gold and five other face-centered-cubic metal crystals, Phys. Rev. E **99**, 022142 (2019).

[46] R. Casalini and T. C. Ransom, On the experimental determination of the repulsive component of the potential from high pressure measurements: What is special about twelve? J. Chem. Phys. **151**, 194504 (2019).

[47] A. Sanz, T. Hecksher, H. W. Hansen, J. C. Dyre, K. Niss, and U. R. Pedersen, Experimental Evidence for a State-Point-Dependent Density-Scaling Exponent of Liquid Dynamics, Phys. Rev. Lett. **122**, 055501 (2019).

[48] R. Casalini and T. C. Ransom, On the pressure dependence of the thermodynamical scaling exponent γ, Soft Matter **16**, 4625 (2020).

[49] M. J. Puska, R. M. Nieminen, and M. Manninen, Atoms embedded in an electron gas: Immersion energies, Phys. Rev. B **24**, 3037 (1981).

[50] J. K. Nørskov, Covalent effects in the effective-medium theory of chemical binding: Hydrogen heats of solution in the 3d metals, Phys. Rev. B **26**, 2875 (1982).

[51] K. W. Jacobsen, P. Stoltze, and J. K. Nørskov, A semi-empirical effective medium theory for metals and alloys, Surf. Sci. **366**, 394 (1996).

[52] S. M. Foiles, M. I. Baskes, and M. S. Daw, Embedded-atom-method functions for the fcc metals Cu, Ag, Au, Ni, Pd, Pt, and their alloys, Phys. Rev. B **33**, 7983 (1986).

[53] M. S. Daw, S. M. Foiles, and M. I. Baskes, The embedded-atom method: A review of theory and applications, Mater. Sci. Rep. **9**, 251 (1993).

[54] N. P. Bailey, T. S. Ingebrigtsen, J. S. Hansen, A. A. Veldhorst, L. Bøhling, C. A. Lemarchand, A. E. Olsen, A. K. Bacher, L. Costigliola, U. R. Pedersen, H. Larsen, J. C. Dyre, and T. B. Schrøder, RUMD: A general purpose molecular dynamics package optimized to utilize GPU hardware down to a few thousand particles, SciPost Phys. **3**, 038 (2017).

[55] K. W. Jacobsen, J. K. Nørskov, and M. J. Puska, Interatomic interactions in the effective-medium theory, Phys. Rev. B **35**, 7423 (1987).

[56] J. K. Nørskov and N. D. Lang, Effective-medium theory of chemical binding: Application to chemisorption, Phys. Rev. B **21**, 2131 (1980).

[57] A. Păduraru, A. Kenoufi, N. P. Bailey, and J. Schiøtz, An interatomic potential for studying CuZr bulk metallic glasses, Adv. Eng. Mater. **9**, 505 (2007).

[58] N. Chetty, K. Stokbro, K. W. Jacobsen, and J. K. Nørskov, *Ab initio* potential for solids, Phys. Rev. B **46**, 3798 (1992).

[59] N. P. Bailey, U. R. Pedersen, N. Gnan, T. B. Schrøder, and J. C. Dyre, Pressure-energy correlations in liquids. I. Results from computer simulations, J. Chem. Phys. **129**, 184507 (2008).

[60] E. Attia, J. C. Dyre, and U. R. Pedersen, An extreme case of density scaling: The Weeks-Chandler-Andersen system at low temperatures, arXiv:2101.10663.

[61] L. Bøhling, T. S. Ingebrigtsen, A. Grzybowski, M. Paluch, J. C. Dyre, and T. B. Schrøder, Scaling of viscous dynamics in simple liquids: Theory, simulation and experiment, New J. Phys. **14**, 113035 (2012).

[62] T. S. Ingebrigtsen, L. Bøhling, T. B. Schrøder, and J. C. Dyre, Thermodynamics of condensed matter with strong pressure-energy correlations, J. Chem. Phys. **136**, 061102 (2012).

[63] J. C. Dyre, Isomorph theory beyond thermal equilibrium, J. Chem. Phys. **153**, 134502 (2020).

[64] D. M. Heyes, D. Dini, L. Costigliola, and J. C. Dyre, Transport coefficients of the Lennard-Jones fluid close to the freezing line, J. Chem. Phys. **151**, 204502 (2019).